Variability of Hawaiian Winter Rainfall during La Niña Events since 1956

CHRISTOPHER F. O'CONNOR AND PAO-SHIN CHU

Department of Atmospheric Sciences, School of Ocean and Earth Science and Technology, University of Hawai'i at Mānoa, Honolulu, Hawaii

PANG-CHI HSU

International Laboratory on Climate and Environment Change and Key Laboratory of Meteorological Disasters of the Ministry of Education, Nanjing University of Information Science and Technology, Nanjing, China

KEVIN KODAMA

Honolulu National Weather Service, Honolulu, Hawaii

(Manuscript received 15 September 2014, in final form 7 July 2015)

ABSTRACT

Rainfall in Hawaii during La Niña years has undergone abnormal variability since the early 1980s. Traditionally, Hawaii receives greater-than-normal precipitation during the La Niña wet seasons. Recently, La Niña years have experienced less-than-normal rainfall. A drying trend in Hawaiian precipitation during La Niña years is evident. A changepoint analysis determined that the shift in precipitation occurred in 1983, forming the two epochs used for comparison in this study. The first epoch (E1) runs from 1956 to 1982 and the second epoch (E2) from 1983 to 2010. Location-specific changes in rainfall anomalies from E1 to E2 throughout the Hawaiian Islands are examined, illustrating that the greatest difference in rainfall between epochs is found on the climatologically drier sides (i.e., south and west) of the islands. Variations in tropical sea surface temperatures and circulation features in the northern Pacific Ocean have changed during La Niña wet seasons, thus changing La Niña–year rainfall.

The strengthening, broadening, and westward shifting of the eastern North Pacific subtropical high, coupled with an eastward elongation and intensification of the subtropical jet stream, are two main influences when considering the lack of precipitation during the recent La Niña wet seasons. Moisture transport analysis shows that variations in circulation structures play a dominant role in the reduction of moisture flux convergence in the Hawaiian region during the second epoch. Additionally, a storm-track analysis reveals that the changes found in the aforementioned circulation features are creating a less favorable environment for the development of Kona lows and midlatitude fronts in the vicinity of Hawaii.

1. Introduction

Pacific island nations are small in size and are often isolated by a vast expanse of ocean. They are highly susceptible to natural disasters and extreme events, including tropical cyclones, droughts, floods, and frequent inundation from high tides. Damages from such extreme events across this region are costly. Many tropical Pacific islands are experiencing rapid population growth, which results in increased demand for water for drinking, food production, and other needs. Further compounding this problem is the great variability of interannual and interdecadal precipitation in this region. Hawaii is particularly vulnerable to extreme precipitation events, which result in flooding, and drought, which leads to lack of usable water and increased risk of fire (Chu et al. 2002). Consecutive dry days across the major Hawaiian Islands have also become longer since 1950s (Chu et al. 2010). Proper planning for extreme events is essential to the well being of these islands, which requires accurate information of climate variability being made available to the government agencies and planners.

Corresponding author address: Christopher F. O'Connor, Department of Atmospheric Sciences, School of Ocean and Earth Science and Technology, University of Hawai'i at Mānoa, 2525 Correa Road, HIG 318, Honolulu, HI 96822.
E-mail: chriso949@gmail.com

DOI: 10.1175/JCLI-D-14-00638.1

The Hawaiian Islands have two distinct seasons, a dry (warm) season and a wet (cool) season. The dry season is from May to October and is dominated by northeasterly trade winds (Garza et al. 2012) resulting from a quasi-stationary subtropical high to the northeast of the state. The main source of rainfall during this time is the lifting of trade winds by the mountainous regions of the islands to produce orographic precipitation systems. Tropical cyclones can also bring precipitation during the dry season; however, extreme rainfall events resulting from tropical cyclones are quite rare to the island chain. The wet season extends from November to April. During this time, normal trade wind patterns are often interrupted by midlatitude fronts, Kona storms, and upper-level disturbances (Ramage 1962; Schroeder 1993). These events cause increased precipitation during the wet season and are quite capable of bringing extreme precipitation to the region. The schematics of major synoptic patterns that produce wet-season rainfall in Hawaii are illustrated in Chu et al. (1993).

Rainfall variability over the Hawaiian Islands is modulated by El Niño–Southern Oscillation (ENSO), which is the leading mode of tropical atmosphere–ocean interaction on interannual time scales. Impacts from such events are felt throughout the entire planet (Trenberth and Caron 2000). ENSO is of most concern for rainfall variability in the tropical Pacific islands on seasonal time scales (Ropelewski and Halpert 1987). Episodes are normally recognized through sea surface temperature (SST) anomalies in the equatorial Pacific region, most commonly in the Niño-3.4 region (5°S–5°N, 120°–170°W). The ENSO events are labeled as either a warm (El Niño) or cold (La Niña) phase, yet its amplitude varies across a continuum with essentially Gaussian statistics (Trenberth 1997). Recent studies have made it apparent that the traditional definition of ENSO episodes is outdated and fails to differentiate between two distinctive types of El Niño episodes. The first, the canonical or eastern Pacific (EP) El Niño, is centered in the eastern equatorial Pacific. The second is the central Pacific (CP) El Niño (Yu and Kao 2007), which is centered farther west. The CP type has also been referred to as the ''El Niño Modoki'' (Ashok et al. 2007). The observed increasing trends of CP events relative to those of EP events (Lee and McPhaden 2010) are noteworthy; however, the cause of the increase is under debate (Newman et al. 2011; Yeh et al. 2011).

In addition to the distinction between EP and CP El Niño events, Trenberth and Stepaniak (2001) support the idea that ENSO may come in many different ''flavors'' that are different from the canonical El Niño and La Niña composites. Johnson (2013) presents a configuration that treats ENSO as a continuum but concludes with a set of the maximum number of statistically distinguishable ENSO patterns. Johnson (2013) uses a neural network–based cluster analysis joined with a statistical distinguishability test, which determines nine unique patterns that characterize the September–February tropical Pacific SST anomaly patterns for the period from 1950 through 2011. These nine patterns represent the flavors of ENSO, which include EP, CP, mixed ENSO neutral patterns, and La Niña events. Over the 1950–2011 period, the most significant trends reflect changes in La Niña patterns. Negative western Pacific warm pool SST anomalies dominate until the mid-1970s during La Niña–like patterns. This tendency is followed by a frequent occurrence of positive western Pacific warm pool SST anomalies, particularly after the mid-1990s. The current study considers the ENSO flavors concept and the shift of SST anomalies during more recent La Niña events to explore the effects of such occurrences on Hawaiian precipitation.

Large-scale circulation mechanisms in the North Pacific have also undergone changes in recent decades. Between 1958 and 1999, He and Gong (2002) found a decadal shift in the western North Pacific subtropical high occurring in about 1979/80. Since 1980, the western North Pacific subtropical high has expanded, strengthened, and moved southwestward. This expansion has led to an increase in precipitation and significant warming in southern China.

In the synoptic-statistical approach to regional downscaling of seasonal rainfall in Hawaii, Timm and Diaz (2009) find that on the western side of Kauai (Fig. 1) the wettest months experience a more relaxed eastern Pacific subtropical high pattern, and vice versa for drier months. In general, most areas of western Kauai receive the majority of their yearly precipitation during the wet season from midlatitude storms. Based on their results, we can conclude that a weaker eastern Pacific subtropical high will promote favorable conditions for midlatitude systems to bring precipitation to the westernmost Hawaiian island.

Hawaii commonly experiences drier-than-normal conditions during El Niño wet seasons (Lyons 1982; Cayan and Peterson 1989; Chu 1989) and greater-than-normal precipitation during the wet season of La Niña years. More specifically, small and positive rainfall amounts are noted from July to October during the El Niño developing years. Deficient rainfall then persists for six consecutive months from November to April of the following year, with a large negative anomaly in January and February (Chu 1995; Chu and Chen 2005). Traditionally, rainfall variations during La Niña events are opposite to that of El Niño, while the largest positive anomaly also occurs in January and February (Chu and Chen 2005).

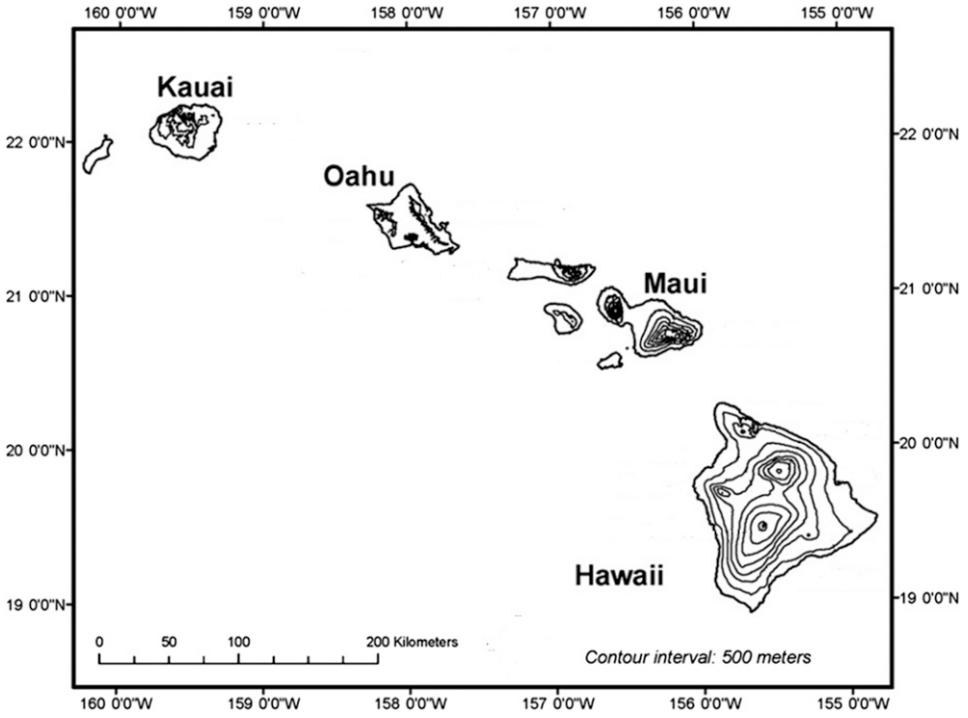

FIG. 1. Orientation map of the Hawaiian Islands; contour interval for elevation is 500 m.

Over the last three decades Hawaii has experienced drier conditions during the wet season (November–April) of La Niña years. The objective of this study is to examine the changes in precipitation in Hawaii during La Niña events since 1956 and to reveal possible causes for such changes. Section 2 describes observational and reanalysis data. In section 3, the methodology for the study is discussed. Section 4 discusses the results from the comparison of rainfall station data between 1956–82 (epoch 1; E1) and 1983–2010 (epoch 2; E2) and negative/positive western North Pacific warm pool SST anomalies, evaluates the circulation features of both epochs, and presents a moisture transport analysis. Furthermore, this section also discusses the implementation of storm-track analysis and explores large-scale winter precipitation patterns in the Pacific from two La Niña events. Section 5 contains the summary and discussion.

2. Data

a. Rainfall data

Monthly precipitation data (TD3220) of Cooperative Observer (COOP) stations are obtained from the National Oceanic and Atmospheric Administration (NOAA)/National Climatic Data Center (NCDC; NCDC 1981). Rainfall data from 50 stations with the best continuity at various elevations and locations (leeward, windward) from the four main islands in the state (Kauai, Oahu, Maui, and Hawaii) are collected (http://rda.ucar.edu/datasets/ds510.0/). The orientation map of the Hawaiian Islands is shown in Fig. 1 (locations of these 50 stations will be displayed later). Because of the high mountains, steep terrain, and the prevailing trade winds, dissimilar locations of rain gauge stations are desirable to ensure that microclimates are well represented, thus avoiding location-dependent bias in the study (Table 1).

The period of study is determined to be 1956–2010 (55 years). The first year in the study is established as 1956 because there is inconsistency in the completeness of the rainfall station data leading up to this year. Prior to 1956, a number of important stations contain large amounts of missing data and are excluded. To hold the wet-season data intact, the water year is defined from July to June of the subsequent year. For example, 1956 means from July 1956 to June 1957, while the 1956 wet season means from November 1956 to April 1957.

b. Oceanic Niño index

La Niña events are determined using the Oceanic Niño index (ONI), from the National Weather Service (NWS) Climate Prediction Center (CPC). Warm (El Niño) and cold (La Niña) episodes are established on a threshold of ±0.5°C for the ONI. This is a 3-month running mean of ERSST.v3b SST anomalies in the

TABLE 1. COOP station wet-season rainfall climatology for 1956–2010. Station ID corresponds with location in Fig. 4. All precipitation values are measured in millimeters. Mean and standard deviation (STD) values are shown for each station.

ID	Station name	Mean (mm)	STD (mm)	ID	Station name	Mean (mm)	STD (mm)
1	Kanalohuluhulu	1258.9	448.8	26	Kalihi Res Site	1611.1	563.7
2	PH Wainiha	1794.2	627.3	27	Waiahole	1836.1	626.9
3	Princeville Ranch	1185.2	370.8	28	Kihei	288.3	176.3
4	Kilauea	1032.0	362.9	29	Puunene	391.2	205.5
5	Waimea	397.2	247.6	30	Kahului Airport	382.8	206.0
6	Makaweli	449.0	238.1	31	Spreckelsville	453.8	218.1
7	Eleele	547.6	253.1	32	Keahua	474.6	222.2
8	Wahiawa	600.9	256.3	33	Paia	546.3	224.2
9	West Lawai	713.1	265.0	34	Hamakuapoko	759.8	279.4
10	Koloa	898.7	318.8	35	Kailua	1741.6	546.2
11	Halenanaho	1101.7	362.6	36	Ulupalakua Ranch	499.9	270.1
12	Puhi	920.7	348.5	37	Kula Hospital	524.8	277.3
13	Lihue Airport	652.7	283.5	38	Haleakala Rng Stn	972.3	535.3
14	Waianae	390.6	233.9	39	Paauilo	1605.4	658.5
15	Honolulu Airport	376.9	223.0	40	Papaikou	2031.8	743.4
16	Moanalua	588.0	242.5	41	Hilo Airport	1843.0	679.9
17	Punchbowl Crater	604.0	234.0	42	Waiakea SCD	2675.8	917.5
18	U. of Hawaii	641.3	260.5	43	Keaau	1991.3	750.2
19	Manoa	1015.9	334.2	44	Lanihau	591.7	256.9
20	Waialae-Kahala	491.5	230.1	45	Kainaliu	525.9	217.0
21	Wilhelmina Rise	743.4	271.6	46	Opihihale 2	467.9	198.6
22	Palolo Valley	1821.1	532.9	47	Naalehu	773.6	370.9
23	Waimanalo Exp F	824.9	342.7	48	Kapapala Ranch	1003.4	505.1
24	Pauoa Flats	2099.4	625.6	49	Hawaii Vol NP HQ	1701.7	635.0
25	Nuuanu Res No. 4	1504.8	503.1	50	Kulani Camp	1729.2	641.3

Niño-3.4 region (Smith et al. 2008). The anomalies are centered on 30-yr base periods updated every 5 years. Cold and warm episodes are defined when the threshold is met for a minimum of five consecutive overlapping seasons. Table 2 lists all La Niña events used in this study.

c. *Circulation data*

The NCEP–NCAR Reanalysis-1 monthly mean data from the NOAA/Earth System Research Laboratory are gathered to perform circulation analysis in the North Pacific region (Kalnay et al. 1996; NCEP reanalysis derived data provided by the NOAA/OAR/ESRL PSD, Boulder, Colorado, http://www.esrl.noaa.gov/psd/, accessed 17 Sep 2014). The dataset consists of 3D atmospheric variables at 17 different pressure levels from 1000 to 10 hPa except for humidity, which was archived from 1000 to 300 hPa. It should be noted that there is a negative trend in the specific humidity in the NCEP–NCAR reanalysis between 1973 and 2007, particularly in the tropical mid- and upper troposphere (Paltridge et al. 2009). Dessler and Davis (2010) noted that the negative trend in the NCEP–NCAR reanalysis is not likely to be realistic when compared to the other four reanalysis products: the 40-yr European Centre for Medium-Range Weather Forecasts (ECMWF) Re-Analysis (ERA-40), the Japanese 25-year Reanalysis Project (JRA-25), the Modern-Era Retrospective Analysis for Research and Applications (MERRA), and the ECMWF interim reanalysis (ERA-Interim). To ensure the validity of our analysis, we performed the same moisture budget analysis using ERA-40 and found that the result is very similar to that based on the NCEP–NCAR reanalysis. Ultimately, we decided to use the NCEP–NCAR reanalysis because of its longer length of record. All fields are at a resolution of 2.5° latitude × 2.5° longitude on a global grid. Individual variables used in this study include geopotential height, specific humidity, and wind and sea level pressure. Reanalysis I data are preferred over the Reanalysis II data, which have a shorter length of record (1979–2013).

3. Methodology

a. *Standardized rainfall data*

All rain gauge data at each individual station are transformed into a standardized anomaly form according to

$$\text{standardized anomaly } (z) = \frac{x - \overline{x}}{s}, \qquad (1)$$

where x is the seasonal rainfall amount for a particular year, $\overline{x}$ is the climatological seasonal mean, and s is the

TABLE 2. List of La Niña events in this study. Wet seasons are defined as November of the designated year through April of the subsequent year. For example, 1956 means from November 1956 to April 1957. The epochs are denoted by 1 or 2 (E1 or E2). The western tropical Pacific SST anomaly throughout the La Niña event is abbreviated as WEPA and negative (positive) anomalies as NA (PA).

La Niña wet seasons	Epoch	WEPA
1956	1	NA
1964	1	NA
1970	1	NA
1971	1	NA
1973	1	NA
1974	1	NA
1975	1	NA
1983	2	PA
1984	2	NA
1988	2	NA
1995	2	PA
1998	2	PA
1999	2	PA
2000	2	PA
2005	2	PA
2007	2	PA
2008	2	PA
2010	2	PA

seasonal standard deviation. The base period is all wet seasons from 1956 to 2010. This transformation ensures that the resultant precipitation series will be dimensionless, and the series holds a mean of zero and a standard deviation of one. Calculated standardized anomalies from all 50 stations are averaged for each wet season. These averaged anomalies are then plotted to detect trends in the precipitation time series. Because of the large number of stations and the seasonal time frame, the averaged anomalies approximately follow a Gaussian distribution. For qualification purposes, the Gaussian distribution is divided into three terciles. According to the standard Gaussian distribution, an anomaly with $Z \leq -0.43$ is in the bottom tercile of the distribution. For this study, a standardized rainfall anomaly falling in the bottom tercile is considered a drier-than-normal season. A standardized rainfall anomaly with $Z \geq 0.43$ is in the top tercile of the distribution and is considered a wetter-than-normal season. Any anomaly satisfying the $-0.43 < Z < 0.43$ is considered to be a normal precipitation season.

As previously described, Johnson (2013) indicated nine individual SST "flavors" in the tropical Pacific during 1950–2011. Of these nine unique SST patterns, La Niña events occur during five of them. Flavors 1, 2, and 5 exhibit negative western tropical Pacific warm pool SST anomalies (NA), while flavors 3 and 4 exhibit positive western tropical Pacific warm pool SST anomalies (PA). The standardized rainfall data from this study are plotted according to the two different western Pacific SST anomaly patterns, NA and PA, in order to reveal the influence of such SST anomaly patterns on Hawaiian precipitation during La Niña events.

Changes in the rainfall data at each individual station throughout the Hawaiian Islands are also considered. The 1956–2010 period is subdivided into two epochs by a changepoint detection analysis described in the following section. The anomalies are averaged for each epoch, resulting in an E1 (before the changepoint) and E2 (after the changepoint) average anomaly value for each station. The difference between E1 and E2 is calculated at each respective location in order to study the changes in rainfall at each station.

b. *Changepoint detection method and hypothesis testing*

The Pettitt–Mann–Whitney method, described fully in the appendix, is used to determine the most likely year of abrupt change in a time series of La Niña events (Mann 1945; Pettitt 1979). Lian et al. (2012) applied this test to identify changepoints in stage and flow time series data from the Illinois River and a portion of the Mississippi River near the junction of both rivers. The changepoint analysis is also utilized by Bassiouni and Oki (2013) to detect a downward shift in streamflow in Hawaii during the twentieth century. The most significant changepoint is found where the significance probability $P(\tau)$ [Eq. (A5)] reaches a maximum. To compare the significance of the difference in the data distribution functions found between E1 and E2, a nonparametric statistical test called the Wilcoxon–Mann–Whitney test is implemented (Chu and Chen 2005).

c. *Moisture transport analysis*

To address what contributes to the decrease in rainfall during recent La Niña years (E2), a column-integrated moisture transport analysis is performed. The horizontal moisture flux, tightly linked with rainfall variation, can be expressed as the sum of moisture convergence and advection. Thus, its epochal changes may be attributed to the changes in both the moisture convergence and horizontal advection, written as

$$\Delta\langle -\nabla\cdot(q\mathbf{V})\rangle = \Delta\langle -q(\nabla\cdot\mathbf{V})\rangle + \Delta\langle -\mathbf{V}\cdot(\nabla q)\rangle, \quad (2)$$

where q is specific humidity ($\mathrm{kg\,kg^{-1}}$), $\mathbf{V}$ is the horizontal vector wind ($\mathrm{m\,s^{-1}}$), the angle brackets $\langle\ \rangle$ indicate a vertical integration from 1000 to 300 hPa, and ∇ is the horizontal gradient operator. The operator Δ represents the difference between epoch 2 and epoch 1 (E2 minus E1). The first term on the right-hand side of

Eq. (2) indicates the effect of moisture convergence, while the second term is the contribution of horizontal moisture advection to the difference of moisture flux between the two epochs.

In the diagnostic case for this study, the contribution of column-integrated moisture convergence is found to be one order of magnitude larger than that of column-integrated moisture advection to the change in total moisture flux (see details in section 4). Because the moisture convergence is modulated by both the circulation and moisture variations, it is worthwhile to further examine the relative roles of dynamic and thermodynamic processes via the following equation

$$-\Delta\langle qD\rangle = -\langle q\Delta D\rangle - \langle \Delta qD\rangle - \langle \Delta q\Delta D\rangle, \qquad (3)$$

where D is divergence (s^{-1}). The first term on the right-hand side of Eq. (3) is associated with the column-integrated circulation change, which can be regarded as a dynamic contributor. The second term involves the column-integrated change in water vapor content holding circulation fixed, thus reflecting the thermodynamic effect. The third term is a nonlinear term that includes the effect of both the column-integrated moisture and circulation changes.

d. Storm-track analysis

After the moisture transport is diagnosed, a storm-track analysis is performed in order to quantifiably measure the contribution of mean circulation changes toward the alteration of specific weather phenomenon between epochs. As stated previously, midlatitude fronts, Kona lows, and upper-level lows are the three main precipitation-bearing systems for the Hawaiian Islands. Kona storms are slow-moving, cutoff lows in the upper-level subtropical westerlies (Ramage 1962). During the wet season, they mainly develop to the northwest of Hawaii with winds coming from the south or southwest and are associated with surface lows. Kona lows last for days, sometimes even more than a week, and may bring flooding to the islands (Kodama and Barnes 1997; Tu and Chen 2011). Reanalysis data of sea level pressure and geopotential height at 250 hPa are analyzed at each daily time step to identify individual systems that potentially bring rainfall to the islands. A storm count is then computed and epoch differences are compared.

A certain criterion is established to achieve this storm count. Systems that reach a predetermined area of study [18.5°–22.5°N, 159.5°–154.5°W (Fig. 1)] are counted and summed for each La Niña winter. Low pressure must show a complete cutoff signature to be considered a Kona low or an upper-level low. To accurately identify Kona lows and upper-level lows, previous relevant literature is investigated (Chu et al. 1993; Otkin and Martin 2004; Caruso and Businger 2006). Morrison and Businger (2001), in their detailed case study of a Kona low, recommend the 250-hPa level as an appropriate height for identifying Kona and upper-level lows. The following precedent is established: a system is considered to be a Kona low formation when the disturbance shows a complete cutoff signature at the surface, as well as in the upper troposphere (250 hPa). Also, the Kona low's center must pass south of 30°N. Upper-level lows are defined when the system shows a complete cutoff signature in the upper troposphere (250 hPa), while lacking one at the surface.

Because of the modification of the midlatitude front by the underlying warm ocean as it approaches Hawaii, the temperature contrast across a frontal system may not be present. Often a frontal system is recognized as a wind shear line and is accompanied by clouds and/or precipitation. For this study, a shear line is defined when a surface level trough extends into the area of study. When a shear line enters the study region, it is tallied as a midlatitude front in the storm count. Disturbances that do not enter the area of Hawaii are not considered.

4. Results

a. Rainfall changes

The average standardized rainfall anomalies during the wet seasons of the La Niña years (Table 2) for the period of 1956–2010 are shown in Fig. 2. The figure shows a drying trend in Hawaiian rainfall. Applying the Pettitt–Mann–Whitney test to the La Niña rainfall data, the most significant changepoint is found in 1983 at the 10% level (p value of 6%), indicating the likelihood of a shift that occurred in 1983. Therefore, E1 runs from 1956 to 1982 and the E2 is from 1983 to 2010. The average standardized rainfall anomalies are also calculated using the two separate epochs together as base periods, which also display a drying trend in precipitation from 1956 to 2010. In other words, the overall trend pattern based on two individual epochs is similar to the one that is derived from the entire epoch (1956–2010). Interestingly, Diaz and Giambelluca (2012) identified multidecadal rainfall variations in the Hawaiian Islands and noted that the period 1947/48 to 1971/72 is the wettest consecutive 25 years while the period 1982/83 to 2006/07 is the driest consecutive 25 years. Therefore, E2 in this study coincides approximately with their driest period. Furthermore, a trend analysis is performed using rainfall of all non–La Niña wet seasons in the study period,

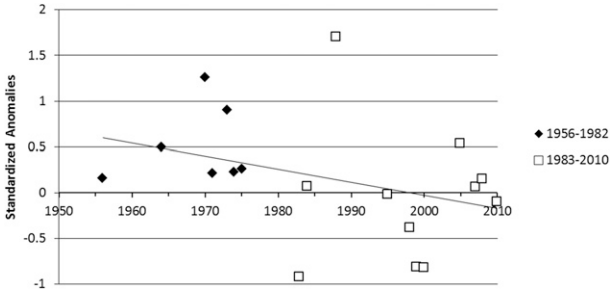

FIG. 2. Standardized rainfall anomalies. La Niña events during E1 (1956–82) and E2 (1983–2010) are marked by black diamonds and open squares, respectively. Note the drying trend indicated by the trend line.

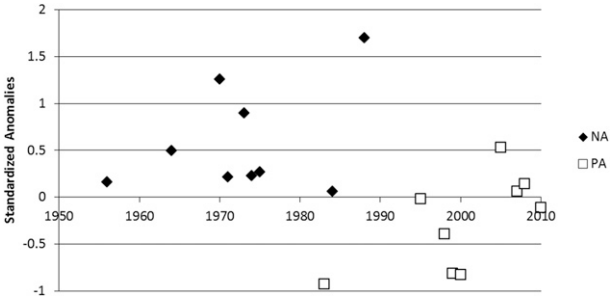

FIG. 3. Standardized rainfall anomalies. The NA cases (negative SST anomalies over the western Pacific warm pool) are denoted in black; PA cases (positive SST anomalies over the western Pacific warm pool) are denoted in open squares.

which provides a flat trend line. There is also an upward trend in ENSO neutral wet-season rainfall and a downward trend in El Niño wet seasons, but none of these trends are statistically significant. This suggests the change of La Niña wet-season rainfall to be the driving factor in the negative trend of Hawaiian precipitation from 1956 to 2010.

All precipitation anomalies in La Niña years are categorized as either normal ($-0.43 < Z < 0.43$), drier than normal ($Z \leq -0.43$), or wetter than normal ($Z \geq 0.43$). During E1 (Fig. 2), positive rainfall anomalies ($Z > 0$) dominate (seven out of seven La Niña cases). Almost half of the standardized rainfall anomalies are wetter than normal (three out of seven occurrences), while the other four are near normal. However, in the second epoch, around half of La Niña events (5 out of 11) show negative rainfall anomalies. Only 18% of the rainfall anomalies are wetter than normal (2 out of 11 occurrences), while 27% of rainfall anomalies are drier than normal (three out of 11 occurrences). While the results presented in Fig. 2 reveal a qualitative shift in La Niña rainfall, the Wilcoxon–Mann–Whitney rank-sum test is performed to test the statistical significance of the shift. The resulting p value of 1.26% suggests that there is a significant difference in La Niña rainfall between E1 and E2 at the 5% level.

Rainfall data are further examined by splitting the dataset into tropical western Pacific SST anomaly patterns, which are categorized as NA and PA by Johnson (2013). The NA patterns dominate in the early portion of the study until about the mid-1980s, after which the PA anomalies prevail (Fig. 3). The wettest La Niña season in this study (1988/89) is characterized by NA anomalies. A strong relationship exists between NA (PA) anomalies and greater-than-normal (less than normal) Hawaiian rainfall. Figure 3 also reveals that the NA anomalies lead to positive rainfall anomalies in Hawaii in nine out of nine occurrences. More than half of these standardized rainfall anomalies are in the upper tercile (five of nine occurrences: 55.6%), while the rest (44.4%) are near normal. Conversely, during PA La Niña events, only 11.1% of the rainfall anomalies are wetter than normal (one out of nine occurrences), while 33.3% of rainfall anomalies are drier than normal (three out of nine occurrences). Of the near-normal rainfall anomalies (five out of nine occurrences) during La Niña years with PA anomalies, two have a positive standardized anomaly, and the remaining three score negative values. The resulting p value of 0.09% implies that there is an extremely strong and significant difference in Hawaiian La Niña rainfall anomalies between positive and negative western Pacific tropical SST anomaly patterns.

We also explore location-dependent changes in the rainfall data for the Hawaiian Islands. Figure 4 displays the relative rainfall differences between E1 and E2 during the La Niña wet season at each of the 50 stations used in this study, as well as the results from the nonparametric significance testing. Decreasing rainfall is highly prominent from E1 to E2 at all island locations. However, a deeper understanding is gained by observing interisland differences. Kauai shows a substantial negative difference in rainfall throughout the island (8 of 13 stations reveal strong decreases). The most outstanding decrease is found on the island of Oahu. Note that 10 of the 14 stations experience a strong negative difference, all of which are significant at the 10% level (eight are significant at the 5% level). On the other hand, the island of Maui shows the smallest decrease in rainfall out of all the islands. None of the Maui stations reveal strong decreases, while 4 of the 11 stations show moderate decreases, and 7 stations express weak decreases. Only one of the rain gauge locations on Maui shows significant change at the 10% level (Kahului Airport).

The island of Hawaii displays a decrease in rainfall at 11 of the 12 stations, while changes in 5 of these 11

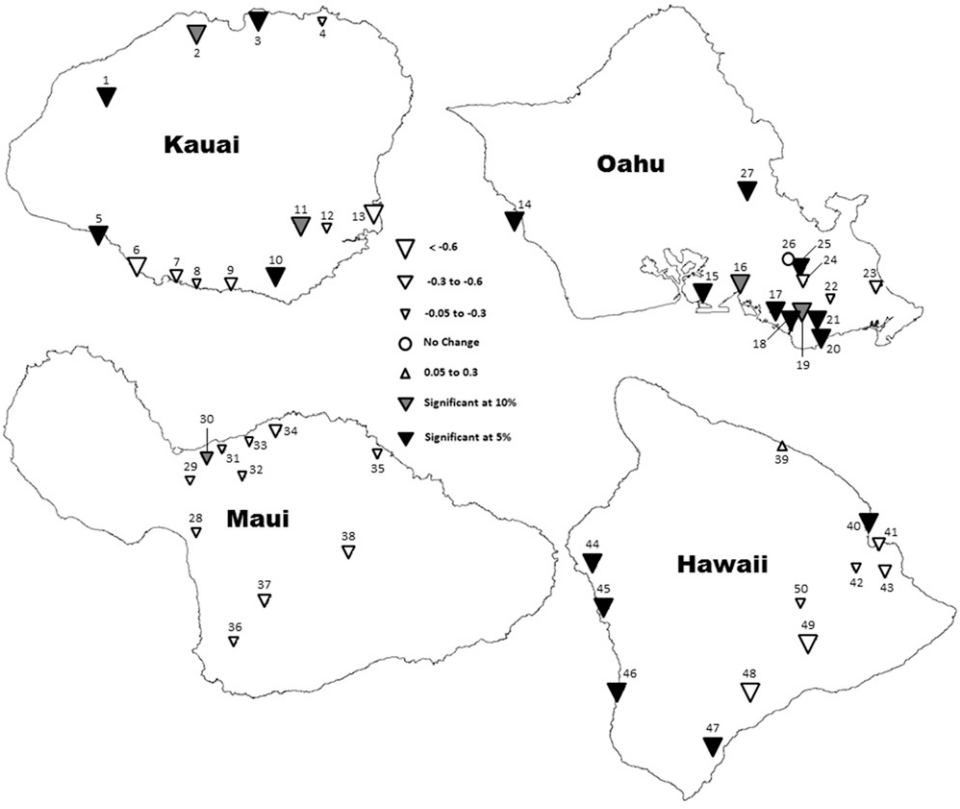

FIG. 4. Epochal difference (E2 − E1) in standardized rainfall anomalies in Hawaii. Rain gauge stations are labeled by triangles and circles. Map legend is in the center of image. Large (medium/small) sized triangles denote strong (moderate/weak) change in rainfall anomalies between epochs. A downward triangle represents a negative difference in rainfall anomaly from E1 to E2. The numerical label next to a station represents the station ID, listed in Table 1. Nonparametric rank-sum test significance is indicated by shading with black (gray) shading representing significant change between epochs at the 5% (10%) level.

stations are statistically significant at the 5% level. The Kona (west) side of the island saw a significant decrease in rainfall from E1 to E2. It is noteworthy to mention that the Kona coast is unique in that more rainfall is observed in summer than in winter. This is caused by the daytime, onshore sea breeze that ascends the mountain slopes and interacts with the descending trade winds through the saddle, producing local orographic showers in the afternoon (Schroeder 1981). The sea breeze circulation is more persistent in summer than in winter, leading to more rainfall in summer along the Kona coast. In the evening, the katabatic land breeze flow dominates the local circulation with few rainfall occurrences (Chen and Nash 1994). Therefore, the large decrease on the Kona coast may not represent a true change in annual rainfall because the wet season analyzed in this study is a dry season on the Kona coast. Interestingly, only one station in Hawaii shows an increase in rainfall, and it is on the northeast side of the island of Hawaii (Paauilo; Fig. 4). From this comparison, we see that the areas where the most extreme difference in rainfall occurs between the two epochs are climatologically drier areas, mostly on the western and southern sides of the island of Hawaii.

b. *Circulation changes*

An examination of NCEP–NCAR Reanalysis I circulation data reveals a few intriguing characteristics that potentially lead to a drying trend in Hawaii from E1 to E2. There are two circulation features that are outstanding during the entire analysis period—the eastern North Pacific subtropical ridge and the North Pacific subtropical jet stream.

Seasonal mean geopotential height at 850 hPa is presented in Fig. 5, which shows a good signature of the eastern North Pacific subtropical ridge as represented by the contour 1540 m. An elongation and strengthening of the subtropical ridge occurs during E2 as seen in Fig. 5b. In the region to the north of Hawaii, the ridge line

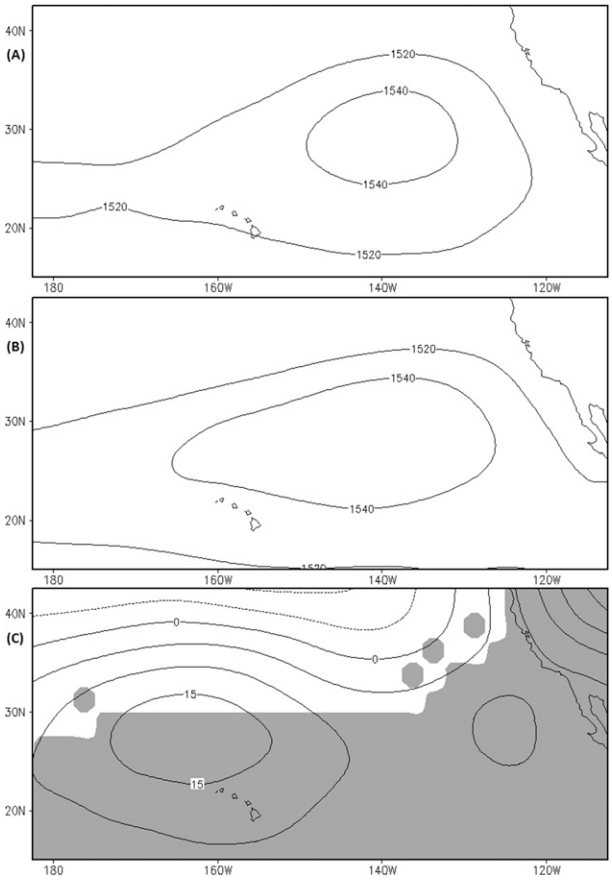

FIG. 5. Seasonal mean geopotential height (m) at 850 hPa during La Niña wet seasons: (a) E1 (1956–82) and (b) E2 (1983–2010). (c) Difference in seasonal mean geopotential height at 850 hPa during La Niña wet seasons, E2 minus E1. The gray-shaded area is where the null hypothesis (two populations have identical distribution functions) of the Wilcoxon–Mann–Whitney rank-sum test was rejected at the 5% level. Solid (dashed) contours denote positive (negative) value, and contour intervals are 5 m.

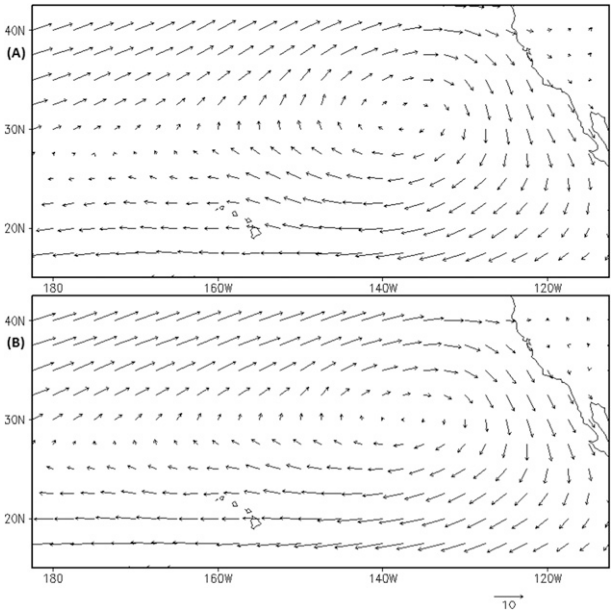

FIG. 6. Seasonal mean wind ($m\,s^{-1}$) at 925 hPa during La Niña wet seasons: (a) E1 (1956–82) and (b) E2 (1983–2010).

stretches westward to approximately 165°W during E2, just to the north of Hawaii. During E1 the westernmost ridgeline retreats eastward at 150°W (Fig. 5a). Figure 5c shows the difference between E1 and E2 and an increase in geopotential height over Hawaii, the subtropical eastern North Pacific, and the western United States during E2. A center of maximum difference in geopotential height is found near Hawaii. The change in geopotential height between the two epochs is significant at the 5% level over the aforementioned regions.

The seasonal mean wind in the lower troposphere (925 hPa) throughout the Hawaiian region experiences a change concomitant to the variation of the subtropical ridge, as shown in Fig. 6. During E1 the wind over Hawaii flows from the east-southeast direction (Fig. 6a). The southerly component is lost during E2, as the wind direction over Hawaii is mainly easterly (Fig. 6b). A southerly tilt in the wind tends to bring an increase in moisture from the south to the state. This result is consistent with Timm and Diaz (2009), who noted an increase in precipitation throughout the islands when a southerly wind anomaly near the surface is present. The opposite can be said for a near-surface northerly wind anomaly, which yields a decrease in precipitation throughout the Hawaiian region. Norton et al. (2011) also found that the meridional wind component at 1000 hPa is one of the key predictors for rainfall variations on Oahu. These relationships are important to reference when considering the outcomes presented in the current study. It is expected that the shifting seasonal mean wind direction in E2, accompanied by the westward elongation of the subtropical ridge, provides the Hawaiian region with less available moisture from the tropics for precipitation events.

Seasonal mean zonal wind (200 hPa) displayed in Fig. 7 indicates a strengthening and extending of the subtropical jet stream core to the east during E2. The easternmost section of the $40\,m\,s^{-1}$ contour touches 178°W in E1 (Fig. 7a), whereas in E2 (Fig. 7b) the same contour line extends farther eastward to 170°W. Similarly, the $60\,m\,s^{-1}$ contour experiences a substantial increase in its east–west radius and overall circumference throughout E2. Figure 7c shows the difference in seasonal mean zonal wind between the two epochs. The elongation of the subtropical jet during the second epoch is significant at the 5% level. This extension of the jet that occurred during E2 places Hawaii closer to

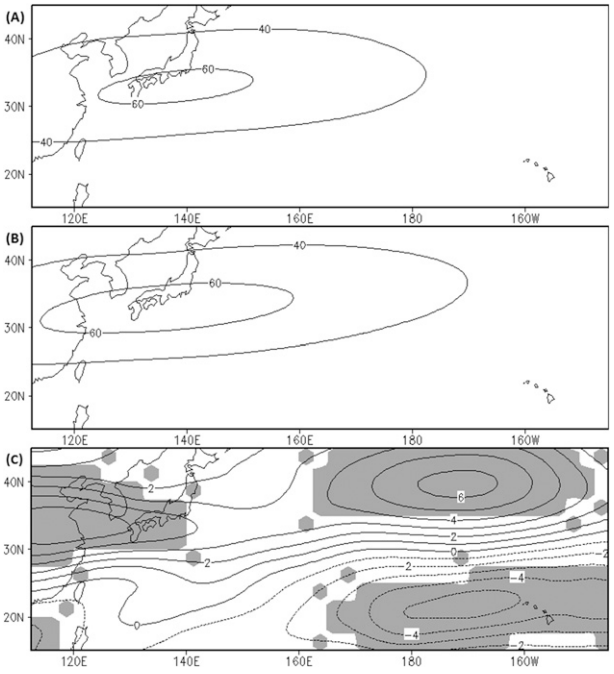

FIG. 7. Seasonal mean zonal wind ($m\,s^{-1}$) at 200 hPa during the La Niña wet seasons: (a) E1 (1956–82) and (b) E2 (1983–2010). The contour intervals are $10\,m\,s^{-1}$. (c) Difference in seasonal mean zonal wind during La Niña wet seasons, E2 minus E1. The gray-shaded area is where the null hypothesis (two populations have identical distribution functions) of the Wilcoxon–Mann–Whitney rank-sum test was rejected at the 5% level. Solid (dashed) contours denote the westerly (easterly) direction.

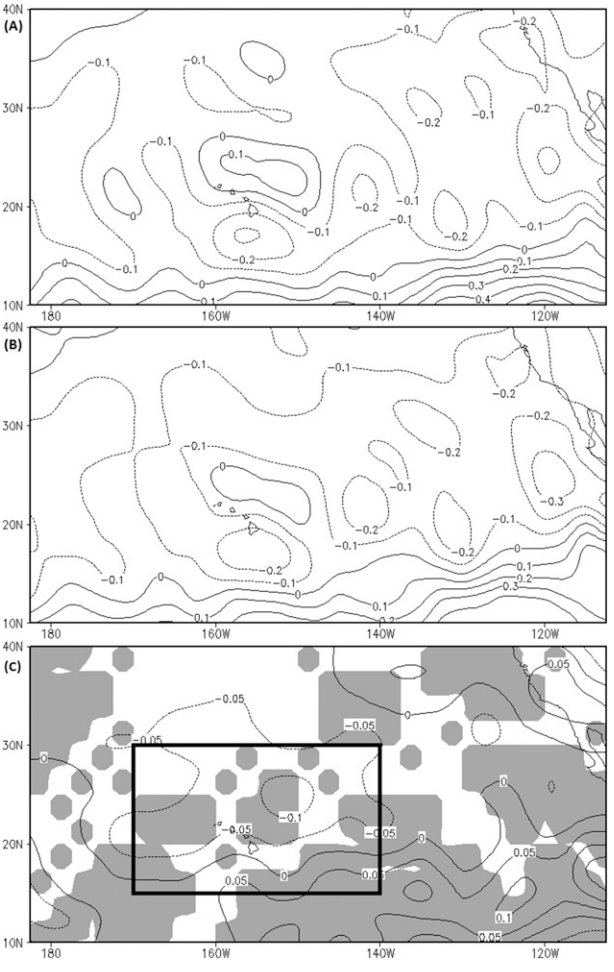

FIG. 8. Column-integrated moisture flux convergence [$-\nabla\cdot(q\mathbf{V})$, unit: $kg\,m^2\,s^{-1}$] during the La Niña wet seasons: (a) E1 (1956–82) and (b) E2 (1983–2010). Solid (dotted) contours denote moisture convergence (divergence). (c) Difference in seasonal mean moisture flux during La Niña wet seasons, E2 minus E1. Solid (dotted) contours denote where difference in seasonal mean moisture flux is positive (negative). The gray-shaded area is where the null hypothesis (two populations have identical distribution functions) of the Wilcoxon–Mann–Whitney rank-sum test was rejected at the 5% level. The solid black box is the domain of Fig. 9.

the right exit region of the jet, bringing increased subsidence and dryness to the region. It is hypothesized that a more zonally elongated waveguide (i.e., the jet stream) would also promote eddy propagation and limit the synoptic-scale wave breaking that leads to cutoff and Kona low formation.

c. *Changes in moisture transport*

A column-integrated (1000–300 hPa) moisture transport analysis is shown in Fig. 8. Investigation of the seasonal mean total moisture flux reveals moisture flux convergence ($-\nabla\cdot q\mathbf{V}>0$) in the region north of Hawaii and in the tropical region (equatorward of 15°N; Figs. 8a,b). Moisture flux divergence is prevalent in the region south of Hawaii and in most of the subtropical Pacific. The difference in moisture flux between the two epochs is shown in Fig. 8c. As anticipated, there is a decrease in moisture flux convergence in the region to the north of Hawaii from E1 to E2. An increase in moisture flux divergence is seen in the region to the south of Hawaii and in most of the central and eastern Pacific subtropical region during E2.

From the total moisture flux equation, the change between epochs in the moisture convergence term is found to be larger than that in moisture advection term (Fig. 9). As a result, we decompose the column-integrated moisture convergence term to examine the role of the dynamic effect (i.e., circulation change), thermodynamic effect (i.e., water vapor content change), and nonlinear effect (i.e., combined influence of moisture and circulation) in contributing to horizontal moisture convergence change throughout the Hawaiian region. Because the focus is on the area surrounding the islands of Hawaii, the moisture convergence analysis is performed for a smaller region bounded by 15°–30°N, 170°–140°W (see the box in Fig. 8c). While the changes between epochs are subtle,

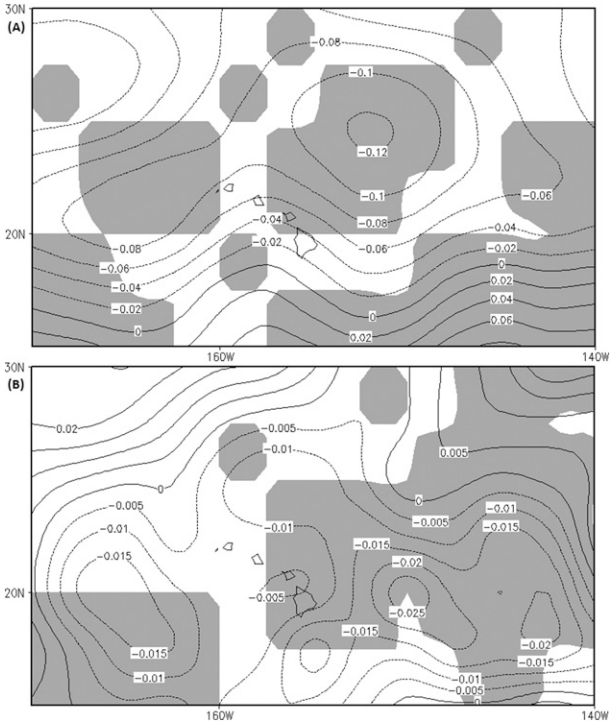

FIG. 9. (a) Difference in column-integrated moisture convergence ($kg\,m^2\,s^{-1}$) between epochs (E2 minus E1) during the La Niña wet seasons. (b) As in (a), but for the difference in column-integrated moisture advection. The domain of this analysis can be seen in Fig. 8c, as depicted by the bold black box. The gray-shaded area is where the null hypothesis (two populations have identical distribution functions) of the Wilcoxon–Mann–Whitney rank-sum test was rejected at the 5% level.

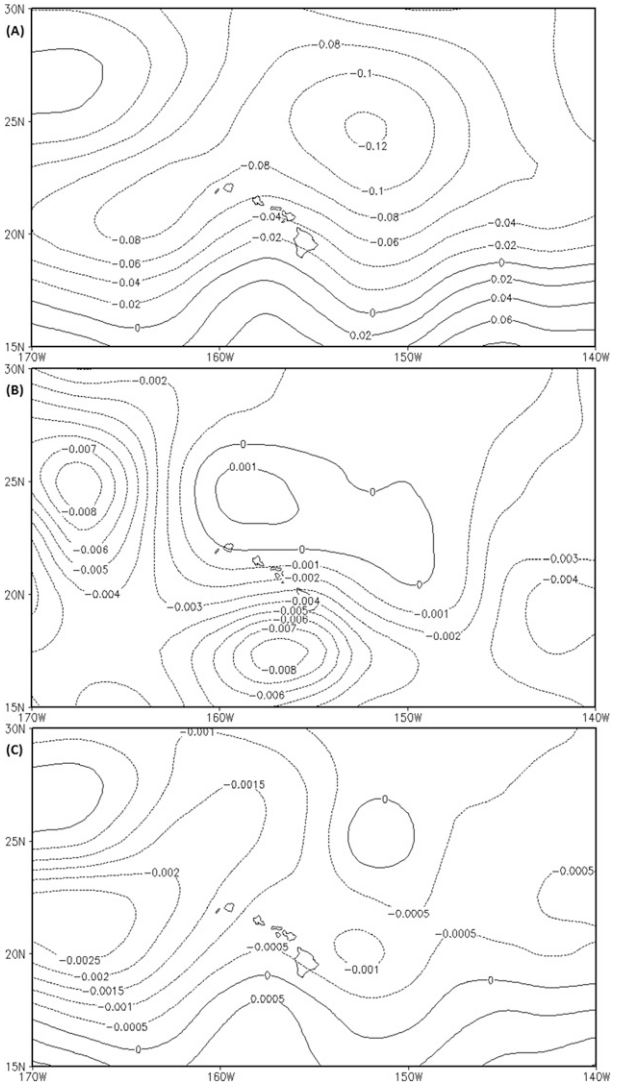

FIG. 10. (a) Difference in column-integrated moisture convergence due to the dynamic effect ($kg\,m^2\,s^{-1}$) between epochs (E2 minus E1) during the La Niña wet seasons. (b),(c) As in (a), but for the difference in column-integrated moisture convergence associated with thermodynamic effect and nonlinear process, respectively. The domain of this analysis can be seen in Fig. 8c, as depicted by the bold black box.

we focus on the areal-averaged difference in magnitude. Figure 10 represents the difference between epochs of the three effects described above. In the Hawaiian region, the area-averaged change attributed to circulation between epochs ($-0.0319\,kg\,m^2\,s^{-1}$; Fig. 10a) is one order of magnitude greater than the difference attributed to thermodynamics ($-0.0025\,kg\,m^2\,s^{-1}$; Fig. 10b) and two orders of magnitude greater than the change presented in the combined influence of moisture and circulation ($-0.000\,46\,kg\,m^2\,s^{-1}$; Fig. 10c). In conclusion, the difference in the dynamic effect between epochs is the primary contributor to the change in moisture transport surrounding Hawaii throughout E2.

d. Changes in storm tracks

Results from the storm-count analysis are shown in Table 3. Generally speaking, each of the three main precipitation-bearing systems occurs at a lower rate during E2 relative to E1. An E2/E1 ratio is calculated for each storm type to weigh the relative magnitude of the decrease. Kona lows show the greatest scaled decrease, as E2 yields 44% fewer Kona lows when compared to E1. While not quite as extreme, midlatitude fronts experience a 23% decrease during E2. Upper-level lows see the smallest difference in occurrence between epochs, yielding an 18% decrease during the second epoch.

The nonparametric rank-sum test is performed on all three datasets, revealing a statistically significant difference in Kona lows and midlatitude fronts between epochs at a nearly 5% level. The change in upper-level lows does not prove to be statistically significant ($p = 45\%$). Therefore, it can be assumed that the

TABLE 3. Storm count by type for each La Niña event in the study. Wet seasons are defined as November of the designated year through April of the subsequent year. Rainfall anomaly is the averaged standardized rainfall value from the 50 Hawaiian stations. Seasons included in E1 (E2) encompass years from 1956 to 1975 (1983 to 2010).

La Niña wet seasons	Midlatitude fronts	Kona lows	Upper-level lows	Rainfall anomaly
1956	15	3	2	0.16
1964	18	5	2	0.50
1970	11	6	8	1.26
1971	9	10	3	0.21
1973	17	5	7	0.90
1974	9	4	6	0.23
1975	14	5	6	0.27
1983	11	2	1	−0.93
1984	13	5	4	0.06
1988	14	3	2	1.70
1995	12	4	3	−0.02
1998	8	1	4	−0.39
1999	6	1	4	−0.81
2000	10	1	2	−0.83
2005	8	4	6	0.53
2007	12	3	6	0.06
2008	8	5	5	−0.11
2010	10	4	7	0.14
E1 Avg	13.3	5.4	4.9	0.50
E2 Avg	10.2	3.0	4.0	−0.05
(E2 − E1)	−3.1	−2.4	−0.9	−0.55
E2/E1	0.77	0.56	0.82	—

enlarging and westward shifting of the eastern Pacific subtropical high, as well as the strengthening and extending of the North Pacific subtropical jet stream during the second epoch, provides less favorable conditions for the development of Kona lows and midlatitude frontal systems in the Hawaiian region. The expansion of the eastern Pacific subtropical high during E2 acts as a blocking mechanism for midlatitude fronts and shear lines, inhibiting these systems from reaching Hawaii. The westward shifting of the eastern Pacific subtropical high also inhibits the surface low formation, which is necessary for Kona low development, in the Hawaiian region. While the upper-level lows do see an average annual decrease during E2, these systems do not succumb to significant declines.

5. Summary and discussion

On an interannual time scale, La Niña events are perceived to bring greater-than-normal seasonal mean precipitation to the Hawaiian Islands during the wet season. However, since the early 1980s, Hawaii has experienced a drying trend in precipitation during La Niña winters. A changepoint analysis is applied to the La Niña rainfall time series during the wet season (November–April) in Hawaii. Results reveal an abrupt shift occurring in 1983, establishing two epochs running from 1956 to 1982 (E1) and 1983 to 2010 (E2). The difference in the rainfall index between the two epochs is significant at the 5% level.

Standardized rainfall data are further examined by splitting the dataset into SST anomaly patterns, revealing a well-defined connection between negative (positive) SST anomalies in the western Pacific warm pool and positive (negative) rainfall anomalies in Hawaii. The nonparametric test also reveals an extremely strong and significant difference in La Niña rainfall between positive and negative western Pacific warm pool SST anomaly patterns. An assessment of location-dependent differences in Hawaiian rainfall station data reveals a noteworthy outcome. The areas exhibiting greatest alteration in rainfall from E1 to E2 are climatologically drier areas on the southern and western sides of the islands. These zones, particularly on Kauai and Oahu, receive most of their rainfall during the wet season from midlatitude weather disturbances.

The eastern North Pacific subtropical ridge and the North Pacific subtropical jet stream are two circulation features that exhibit changes. Evaluating seasonal mean geopotential height at 850 hPa exposes a westward elongation and strengthening of the subtropical ridge occurring during E2. Seasonal mean wind in the lower troposphere (925 hPa) throughout the Hawaiian region experiences a change concurrent to the variation of the

subtropical ridge, with wind direction shifting from east-southeasterly in E1 to easterly in E2. This shift in wind direction implies less total water available present in E2, as moisture-laden air to the south of Hawaii is more restricted from reaching the islands. The seasonal mean zonal wind in the upper troposphere indicates a strengthening and eastward extension of the subtropical jet stream to 170°W during the second epoch. This stretching positions Hawaii closer to the right exit region of the jet, which promotes subsidence and dryness.

A column-integrated moisture transport analysis reveals a decrease in moisture flux convergence in the region north of Hawaii in the most recent epoch. An increase of moisture flux divergence is seen in the region south of Hawaii and in most of the central Pacific subtropical region during E2. We discover that the horizontal moisture convergence term ($-q\nabla \cdot \mathbf{V}$) is the main factor for the difference in moisture flux. This term is further investigated to examine the role of the dynamic effect, thermodynamic effect, and nonlinear effect in contribution. The change in the circulation term (i.e., dynamic effect) between epochs is found to be the primary contributor to the difference in moisture surrounding Hawaii throughout E2.

For the first time, individual midlatitude fronts, Kona lows, and upper-level lows, which enter the Hawaiian region, are counted and totaled for each La Niña wet season since 1956. Results indicate that Kona lows and midlatitude fronts feel the most drastic change during E2, and such differences are determined to be statistically significant. Upper-level lows do not experience such an extreme change between epochs. Therefore, it can be assumed that the declining occurrence of Kona lows and midlatitude fronts contribute mainly to a decrease in La Niña precipitation since 1983 throughout the Hawaiian region.

While the real causes of the decadal-scale change in the La Niña–Hawaii precipitation since 1983 are not clear, it is hypothesized that the regime shift of 1976/77 over the North Pacific and other oceans or a phase change in the Pacific decadal oscillation (PDO) around 1976/77 (Zhang et al. 1997; Mantua et al. 1997) may be instrumental for such a change. The PDO appears to exert a modulating effect on ENSO teleconnections (e.g., Gershunov and Barnett 1998). Note that in Table 2, the last La Niña event before 1983 in E2 occurred in 1975 during E1.

Trenberth and Hurrell (1994) showed a deeper Aleutian low pressure system and an attendant southward shift in storm tracks over the North Pacific from about 1976 to 1988. Kumar et al. (2004) likewise noted an upward trend in the sea surface temperature over most of the global oceans, with the most abrupt shift occurring around 1976. Through observations and numerical simulations, Kumar et al. (2010) demonstrated drastic changes in the La Niña teleconnections patterns for the pre-1980 and post-1980 periods. Independently, Chu and Chen (2005) studied changes in Hawaiian rainfall during El Niño and La Niña years on the interdecadal time scales. They noted that the deepening of the Aleutian low is accompanied by a band of enhanced surface westerly anomalies to the north of Hawaii when the composite of La Niña events that occurred prior to 1976 is subtracted from the composite of El Niño events after 1976. Diaz and Giambelluca (2012) found a similar feature in the North Pacific circulation associated with the Aleutian low on the multidecadal time scales (25-yr interval). The strong surface westerlies weaken the climatological easterly trade winds over the subtropical central North Pacific, implying a reduction in trade wind rainfall. In addition, anomalous and deep sinking motion over Hawaii hinders the development of subtropical cyclones and upper-level lows and passage of midlatitude frontal systems to the Hawaiian Islands between the composite of two extreme climatic events (Chu and Chen 2005). It is inferred from these features, together with the reduced trade winds, that Hawaii would experience low La Niña precipitation since 1983.

The results presented in this study may benefit the many agencies that are concerned with forecasting precipitation for Hawaii winter seasons during La Niña events. For instance, the National Weather Service of Honolulu produces seasonal precipitation predictions for the islands of Hawaii. Because many people (e.g., farmers, hydrologists, and city and county planners) rely on these forecasts, improving the accuracy of such predictions is vital to the well being of broader sectors in Hawaii. Also, because the La Niña events are perceived to bring excess rainfall to the state, the lesser-known possibility of decreased rainfall during these events in recent decades must be publicized so that proper planning and hydrological management can ensue. Such information is highly valuable for other tropical Pacific island communities that may be feeling similar changes in seasonal rainfall trends. The method performed in this study can be implemented for any specific area in order to obtain an accurate depiction of possible rainfall climates, especially those that have experienced a change in precipitation during recent La Niña events.

Acknowledgments. We thank Dr. Andre Marquez, Christopher Holloway, Kristine Tofte, and Christopher Wrenn for their stimulating discussions and critiques. Oliver Timm assisted in a preliminary review, while May Izumi served as the editor. We are indebted to the insightful and detailed comments from three reviewers which have improved the presentation of this paper considerably. Christopher O'Connor is funded by the

Hawaii State Climate Office through SOEST at the University of Hawai'i at Mānoa. P.-C. Hsu is supported by NSFC Grant 41375100, Natural Science Foundation of Jiangsu Province (BK20140046), and Research Project of Chinese Ministry of Education (213014A).

APPENDIX

Pettitt–Mann–Whitney Method: A Changepoint Analysis

A time series with length n, and the most likely changepoint given by τ, is divided into two sample groups represented by $X_1, X_2, \ldots, X_{\tau-1}$ and $X_\tau, X_{\tau+1}, \ldots, X_n$. Now consider the problem of testing a null hypothesis (H_0) of "no change" against the alternative hypothesis (H_A) of "change." That is, the null hypothesis would be two identical distribution functions. Pettitt (1979) showed how a version of the nonparametric Mann–Whitney two-sample test (Mann 1945) can be modified for the changepoint problem. The following indices $V(t)$ and $U(t)$ are then calculated from

$$V_{t,n} = \sum_{j=1}^{n} \operatorname{sgn}(X_t - X_j) \quad \text{for} \quad t = 1, n, \tag{A1}$$

$$U_{t,n} = U_{t-1,n} + V_{t,n} \quad \text{for} \quad t = 2, n, \tag{A2}$$

and

$$U_{1,n} = V_{1,n}, \tag{A3}$$

where $\operatorname{sgn}(x)$ in Eq. (A1) is defined as follows:

$$\operatorname{sgn}(x) = \begin{cases} 1, x > 0 \\ 0, x = 0 \\ -1, x < 0 \end{cases}. \tag{A4}$$

The approximate significance probability $P(\tau)$ for a changepoint is

$$P(\tau) = 1 - \exp\left[-\frac{6U_{t,n}^2}{(n^3 + n^2)}\right]. \tag{A5}$$

The most significant changepoint is found where the significance probability $P(\tau)$ reaches a maximum. This test is applied to standardized rainfall values to find the most probable changepoint in the period of this study.

REFERENCES

Ashok, K., S. K. Behera, S. A. Rao, H. Weng, and T. Yamagata, 2007: El Niño Modoki and its possible teleconnection. *J. Geophys. Res.*, **112**, C11007, doi:10.1029/2006JC003798.

Bassiouni, M., and D. S. Oki, 2013: Trends and shifts in streamflow in Hawai'i, 1913–2008. *Hydrol. Processes*, **27**, 1484–1500, doi:10.1002/hyp.9298.

Caruso, S. J., and S. Businger, 2006: Subtropical cyclogenesis over the central North Pacific. *Wea. Forecasting*, **21**, 193–205, doi:10.1175/WAF914.1.

Cayan, D. R., and D. H. Peterson, 1989: The influence of North Pacific atmospheric circulation on streamflow in the West. *Aspects of Climate Variability in the Pacific and the Western Americas*, *Geophys. Monogr.*, Vol. 55, 375–397.

Chen, Y.-L., and A. J. Nash, 1994: Diurnal variation of surface airflow and rainfall frequencies on the island of Hawaii. *Mon. Wea. Rev.*, **122**, 34–56, doi:10.1175/1520-0493(1994)122<0034:DVOSAA>2.0.CO;2.

Chu, P.-S., 1989: Hawaiian drought and the Southern Oscillation. *Int. J. Climatol.*, **9**, 619–631, doi:10.1002/joc.3370090606.

——, 1995: Hawaii rainfall anomalies and El Niño. *J. Climate*, **8**, 1697–1703, doi:10.1175/1520-0442(1995)008<1697:HRAAEN>2.0.CO;2.

——, and H. Chen, 2005: Interannual and interdecadal rainfall variations in the Hawaiian Islands. *J. Climate*, **18**, 4796–4813, doi:10.1175/JCLI3578.1.

——, A. J. Nash, and F. Porter, 1993: Diagnostic studies of two contrasting rainfall episodes in Hawaii: Dry 1981 and wet 1982. *J. Climate*, **6**, 1457–1462, doi:10.1175/1520-0442(1993)006<1457:DSOTCR>2.0.CO;2.

——, W. Yan, and F. Fujioka, 2002: Fire-climate relationships and long-lead wildfire prediction for Hawaii. *Int. J. Wildland Fire*, **11**, 25–31, doi:10.1071/WF01040.

——, Y. R. Chen, and T. A. Schroeder, 2010: Changes in precipitation extremes in the Hawaiian Islands in a warming climate. *J. Climate*, **23**, 4881–4900, doi:10.1175/2010JCLI3484.1.

Dessler, A. E., and M. Davis, 2010: Trends in tropospheric humidity from reanalysis systems. *J. Geophys. Res.*, **115**, D19127, doi:10.1029/2010JD014192.

Diaz, H. F., and T. W. Giambelluca, 2012: Changes in atmospheric circulation patterns associated with high and low rainfall regimes in the Hawaiian Islands region on multiple time scales. *Global Planet. Change*, **98-99**, 97–108, doi:10.1016/j.gloplacha.2012.08.011.

Garza, J., P.-S. Chu, C. Norton, and T. A. Schroeder, 2012: Changes of the prevailing trade winds over the Islands of Hawaii and the North Pacific. *J. Geophys. Res.*, **117**, D11109, doi:10.1029/2011JD016888.

Gershunov, A., and T. P. Barnett, 1998: Interdecadal modulation of ENSO teleconnections. *Bull. Amer. Meteor. Soc.*, **79**, 2715–2725, doi:10.1175/1520-0477(1998)079<2715:IMOET>2.0.CO;2.

He, X.-Z., and D.-Y. Gong, 2002: Interdecadal change in western Pacific subtropical high and climatic effects. *J. Geogr. Sci.*, **12**, 202–209, doi:10.1007/BF02837475.

Johnson, N., 2013: How many ENSO flavors can we distinguish? *J. Climate*, **26**, 4816–4827, doi:10.1175/JCLI-D-12-00649.1.

Kalnay, E., and Coauthors, 1996: The NCEP/NCAR 40-Year Reanalysis Project. *Bull. Amer. Meteor. Soc.*, **77**, 437–471, doi:10.1175/1520-0477(1996)077<0437:TNYRP>2.0.CO;2.

Kodama, K. R., and G. M. Barnes, 1997: Heavy rain events over the south-facing slopes of Hawaii: Attendant conditions. *Wea. Forecasting*, **12**, 347–367, doi:10.1175/1520-0434(1997)012<0347:HREOTS>2.0.CO;2.

Kumar, A., F. Yang, L. Goddard, and S. Schubert, 2004: Differing trends in the tropical surface temperatures and precipitation

over land and oceans. *J. Climate*, **17**, 653–664, doi:10.1175/1520-0442(2004)017<0653:DTITTS>2.0.CO;2.

——, B. Jha, and M. L'Heureux, 2010: Are tropical SST trends changing the global teleconnection during La Niña? *Geophys. Res. Lett.*, **37**, L12702, doi:10.1029/2010GL043394; Corrigendum, **39**, L21709, doi:10.1029/2012GL054139.

Lee, T., and M. J. McPhaden, 2010: Increasing intensity of El Niño in the central-equatorial Pacific. *Geophys. Res. Lett.*, **37**, L14603, doi:10.1029/2010GL044007.

Lian, Y., J.-Y. You, R. Sparks, and M. Demissie, 2012: Impact of human activities to hydrologic alterations on the Illinois River. *J. Hydrol. Eng.*, **17**, 537–546, doi:10.1061/(ASCE)HE.1943-5584.0000465.

Lyons, S. W., 1982: Empirical orthogonal function analysis of Hawaiian rainfall. *J. Appl. Meteor.*, **21**, 1713–1729, doi:10.1175/1520-0450(1982)021<1713:EOFAOH>2.0.CO;2.

Mann, H. B., 1945: Non-parametric test against trends. *Econometrica*, **13**, 245–259, doi:10.2307/1907187.

Mantua, N. J., S. R. Hare, Y. Zhang, J. M. Wallace, and R. C. Francis, 1997: A Pacific interdecadal climate oscillation with impacts on salmon production. *Bull. Amer. Meteor. Soc.*, **78**, 1069–1079, doi:10.1175/1520-0477(1997)078<1069:APICOW>2.0.CO;2.

Morrison, I., and S. Businger, 2001: Synoptic structure and evolution of a Kona low. *Wea. Forecasting*, **16**, 81–98, doi:10.1175/1520-0434(2001)016<0081:SSAEOA>2.0.CO;2.

NCDC, 1981: NCDC TD3200 U.S. cooperative summary of day, 1890(1948)-cont. Research Data Archive at NCAR, accessed 17 September 2014. [Available online at http://rda.ucar.edu/datasets/ds510.0/.]

Newman, M., S. I. Shin, and M. A. Alexander, 2011: Natural variation in ENSO flavors. *Geophys. Res. Lett.*, **38**, L14705, doi:10.1029/2011GL047658.

Norton, C., P.-S. Chu, and T. A. Schroeder, 2011: Estimating changes in future heavy rainfall events for Oahu, Hawaii: A statistical downscaling approach. *J. Geophys. Res.*, **116**, D17110, doi:10.1029/2011JD015641.

Otkin, J. A., and J. E. Martin, 2004: A synoptic climatology of the subtropical Kona storm. *Mon. Wea. Rev.*, **132**, 1502–1517, doi:10.1175/1520-0493(2004)132<1502:ASCOTS>2.0.CO;2.

Paltridge, G., A. Arking, and M. Pook, 2009: Trends in middle- and upper-tropospheric humidity from NCEP reanalysis data. *Theor. Appl. Climatol.*, **98**, 351–359, doi:10.1007/s00704-009-0117-x.

Pettitt, A. N., 1979: A non-parametric approach to the change-point detection. *Appl. Stat.*, **28**, 126–135, doi:10.2307/2346729.

Ramage, C. S., 1962: The subtropical cyclone. *J. Geophys. Res.*, **67**, 1401–1411, doi:10.1029/JZ067i004p01401.

Ropelewski, C. F., and M. S. Halpert, 1987: Global and regional scale precipitation patterns associated with the El Niño/Southern Oscillation. *Mon. Wea. Rev.*, **115**, 1606–1626, doi:10.1175/1520-0493(1987)115<1606:GARSPP>2.0.CO;2.

Schroeder, T. A., 1981: Characteristics of local winds in northwest Hawaii. *J. Appl. Meteor.*, **20**, 874–881, doi:10.1175/1520-0450(1981)020<0874:COLWIN>2.0.CO;2.

——, 1993: Climate controls. *Prevailing Trade Winds*, M. Sanderson, Ed., University of Hawaii Press, 12–36.

Smith, T. M., R. W. Reynolds, T. C. Peterson, and J. Lawrimore, 2008: Improvements to NOAA's historical merged land-ocean surface temperature analysis (1880–2006). *J. Climate*, **21**, 2283–2296, doi:10.1175/2007JCLI2100.1.

Timm, O., and H. F. Diaz, 2009: Synoptic-statistical approach to regional downscaling of IPCC twenty-first-century climate projections: Seasonal rainfall over the Hawaiian Islands. *J. Climate*, **22**, 4261–4280, doi:10.1175/2009JCLI2833.1.

Trenberth, K. E., 1997: The definition of El Niño. *Bull. Amer. Meteor. Soc.*, **78**, 2771–2777, doi:10.1175/1520-0477(1997)078<2771:TDOENO>2.0.CO;2.

——, and J. W. Hurrell, 1994: Decadal atmosphere-ocean variations in the Pacific. *Climate Dyn.*, **9**, 303–319, doi:10.1007/BF00204745.

——, and J. M. Caron, 2000: The Southern Oscillation revisited: Sea level pressures, surface temperatures, and precipitation. *J. Climate*, **13**, 4358–4365, doi:10.1175/1520-0442(2000)013<4358:TSORSL>2.0.CO;2.

——, and D. P. Stepaniak, 2001: Indices of El Niño evolution. *J. Climate*, **14**, 1697–1701, doi:10.1175/1520-0442(2001)014<1697:LIOENO>2.0.CO;2.

Tu, C.-C., and Y.-L. Chen, 2011: Favorable conditions for the development of a heavy rainfall event over Oahu during the 2006 wet period. *Wea. Forecasting*, **26**, 280–300, doi:10.1175/2010WAF2222449.1.

Yeh, S.-W., B. Kirtman, J.-S. Kug, W. Park, and M. Latif, 2011: Natural variability of the central Pacific El Niño event on multi-centennial timescales. *Geophys. Res. Lett.*, **38**, L02704, doi:10.1029/2010GL045886.

Yu, J.-Y., and H.-Y. Kao, 2007: Decadal changes of ENSO persistence barrier in SST and ocean heat content indices: 1958–2001. *J. Geophys. Res.*, **112**, D13106, doi:10.1029/2006JD007654.

Zhang, Y., J. M. Wallace, and D. S. Battisti, 1997: ENSO-like interdecadal variability: 1900–93. *J. Climate*, **10**, 1004–1020, doi:10.1175/1520-0442(1997)010<1004:ELIV>2.0.CO;2.